NANO LETTERS

pubs.acs.org/NanoLett

Surface-Initiated Assembly of Protein Nanofabrics

Adam W. Feinberg, and Kevin Kit Parker*

Disease Biophysics Group, Wyss Institute for Biologically-Inspired Engineering, School of Engineering and Applied Sciences, Harvard University, Cambridge, Massachusetts 02138

ABSTRACT Cells and tissues are self-organized within an extracellular matrix (ECM) composed of multifunctional, nano- to micrometer scale protein fibrils. We have developed a cell-free, surface-initiated assembly technique to rebuild this ECM structure in vitro. The matrix proteins fibronectin, laminin, fibrinogen, collagen type I, and collagen type IV are micropatterned onto thermosensitive surfaces as 1 to 10 nm thick, micrometer to centimeter wide networks, and released as flexible, free-standing nanofabrics. Independent control of microstructure and protein composition enables us to engineer the mechanical and chemical anisotropy. Fibronectin nanofabrics are highly extensible (>4-fold) and serve as scaffolds for engineering synchronously contracting, cardiac muscle; demonstrating biofunctionality comparable to cell-generated ECM.

KEYWORDS Extracellular matrix protein, fibronectin, laminin, nanofiber, soft lithography, cardiac, tissue engineering

The extracellular matrix (ECM) is a heterogeneous protein network that provides structural support, spatial organization, and functional integration of cells and tissues. Specific molecular domains within the ECM proteins regulate supramolecular assembly (fibrillogenesis),[1,2] cell adhesion,[3] and cell-signaling by transducing mechanical forces and regulating the activity of growth factors.[4−6] Cells synthesize, spatially arrange, and mechanochemically couple the ECM that surrounds them,[7−11] typically via a receptor-mediated nanoscale assembly process.[1,2] The ability to recapitulate ECM networks would allow the design of biomimetic materials and provide novel tissue engineering scaffolds for the study of development,[7,12] disease[8] and tissue regeneration.[10,11,13] However, it has proven challenging to de novo engineer the complex topology and composition of ECM networks in cell-free systems.

To address this need, we considered how cells build the ECM and developed a biologically inspired approach to mimic it. ECM proteins are secreted by cells as multimeric molecules that undergo a conformational change to expose cryptic protein−protein binding domains during fibrillogenesis. Fibronectin (FN) fibrillogenesis is considered a paradigm for matrix assembly and is the initial ECM protein expressed in wound healing and embryonic development.[14] Cells use integrin receptors to bind FN homodimers, then use the contracting actin cytoskeleton (i.e., force) to cluster, unfold, and assemble the dimers into insoluble fibrils.[1,2] This receptor-mediated process enables cells to build the ECM around themselves, organize the matrix structure from the nanometer to tissue-scale, and release it from the cell surface. Fibrillogenesis in a cell-free, in vitro system is possible using denaturants[15] or reducing agents[16] to induce assembly in solution by exposing cryptic domains, but the random matrix that results has no structural organization. Improved control has been achieved using force-based assembly, where FN self-assembles into fibrillar networks on dipalmitoyl phosphatidylcholine (DPPC) monolayers under tension,[17] forms microscale FN fibrils drawn from FN droplets,[18,19] generates nanoscale FN fibrils by dewetting FN solutions from microengineered surfaces[20] and produces tubular FN mats on the shafts of high-speed motors due to shear force.[21] This demonstrates that interfacial molecular forces (e.g., surface energy, surface tension, shear force) can nucleate and drive fibrillogenesis. However, these approaches are limited to a small set of protein-types and planar geometries permanently bound to surfaces, though recent advances have enabled the transfer of engineered ECM between surfaces.[22] We sought to apply interface driven assembly more broadly to engineer matrix architecture and composition at the nanoscale with multiple ECM proteins and with the key ability to create free-standing matrix structures.

Here we show that protein−surface interactions (i.e., surface energy) can be used to unfold ECM proteins in lieu of surface tension[17,18,20] or shear force,[21] and trigger protein assembly by dissolution of the supporting substrate. The process, termed surface-initiated assembly, is achieved by (i) adsorbing nanometer-thick layers of ECM proteins from solution onto a hydrophobic surface at high density to partially unfold them and expose cryptic binding domains,[23,24] (ii) transferring the ECM proteins in the unfolded state to a relatively hydrophilic, dissolvable surface, and (iii) thermally triggering surface dissolution to synchronize matrix assembly and nondestructive release (Figure 1, see the Supporting Information for more detail). FN and other serum

* To whom correspondence should be addressed. E-mail: kkparker@seas.harvard.edu.

Received for review: 03/21/2010
Published on Web: 05/20/2010

DOI: 10.1021/nl100998p | *Nano Lett.* **2010,** *10,* 2184–2191

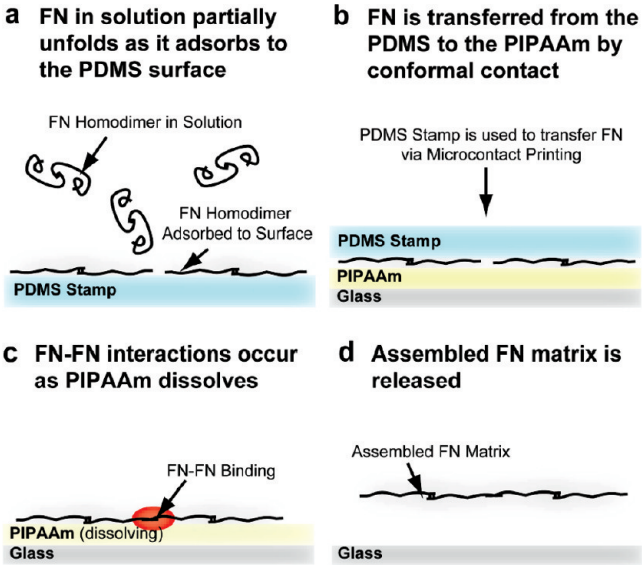

FIGURE 1. A schematic showing the proposed method by which FN homodimers undergo surface-initiated assembly. (a) Soluble FN homodimers in solution adsorb onto PDMS and partially unfold (denature) due to hydrophobic surface interactions. (b) The PDMS surface (typically a stamp for microcontact printing) is placed in conformal contact with a PIPAAm film transferring a portion of the unfolded FN from one surface to the other. (c) The FN on the PIPPAm is hydrated in 37 °C water and then cooled to <35 °C to cause PIPAAm dissolution. (d) As the PIPAAm completely dissolves the assembled FN nanofabric is released as an insoluble, supramolecular structure.

proteins denature onto hydrophobic and hydrophilic polymeric surfaces,[25] unfolding from the globular, solution conformations into extended, rodlike conformations.[23,26,27] Surface-initiated assembly leverages this phenomenon in combination with soft lithography to create hierarchically structured, fibrillar networks; experimentally verified for FN, laminin (LAM), fibrinogen (FIB), collagen type I (COL_I), collagen type IV (COL_{IV}) and combinations thereof. This suggests that unfolded ECM proteins were at sufficient density, conformation, and molecular mobility to bind during substrate dissolution. Exactly how and when assembly occurs may differ depending on the ECM protein. Here we focus our study on the capability of this technique to build free-standing, protein-based materials with unique composition, architectures, mechanical properties and biological activity.

We engineered hierarchical protein matrices, termed protein nanofabrics, by spin coating an anhydrous poly(*N*-isopropylacrylamide) (PIPAAm) film onto glass coverslips onto which ECM proteins were deposited in spatially defined patterns by microcontact printing (μCP) with polydimethylsiloxane (PDMS) stamps (Figure 2a).[13,28−31] Complete ECM release and PIPAAm dissolution was achieved by using linear PIPAAm chains,[13] avoiding the interchain cross linking commonly used for cell-sheet engineering.[32,33] By properly templating the μCP protein array, the ECM was released from the surface as ribbon- and fabriclike structures. The μCP process step may be repeated multiple times with multiple proteins in multiple geometries to produce interconnected nanofabrics with variable thread counts and weaves, rip-stop properties and both chemical and mechanical anisotropy.

As proof-of-concept we engineered protein nanofabrics from a range of ECM proteins. We patterned 20 μm wide protein lines with 20 μm spacing (20 × 20), 15 μm wide lines with 15 μm spacing (15 × 15), and 10 μm wide lines with 10 μm spacing (10 × 10) to demonstrate the capability to tailor the nanofabric structure. For example, 20 × 20 FN lines were patterned on PIPAAm once to create discrete lines (Figure 2b), or repeatedly and at various angles (e.g., 23, 43, and 90°) to vary the nanofabric weave (Figure 2c−e, respectively). The serially printed 20 × 20 FN lines adhered to one another after release and maintained the as-patterned geometry (90°, Figure 2e), indicating that intermolecular bonds formed between layers. Nanofabric architecture was tailored by changing the stamp geometry and/or the orientation of serial stampings, as interconnected FN nanofabrics could also be formed with a single stamp (Figure 2f). Micron-scale protein patterning with μCP was reproducible, where infrequent defects were due only to dust particulates trapped between the PDMS stamp and the PIPAAm during patterning, causing circular holes in the resulting nanofabric (Supporting Information, Figure S1),

Surface-initiated assembly is compatible with multiple ECM proteins, including LAM, FIB, COL_I, COL_{IV}, and their combinations. For example, LAM and FN were integrated into a single, chemically and mechanically anisotropic nanofabric by serially patterning 20 × 20 FN lines and 20 × 20 LAM lines at 90° (Figure 2g−i) with regions of uniform protein type (Figure 2j) and rolled into larger-scale fibers with subdomains of FN and LAM (Figure 2k). Specific FN-LAM binding with the ability to bear stress was evidenced by rip-stop like support of small tears (Figure 2i). LAM nanofabrics were also fabricated without the presence of FN (Figure 2l). Similarly, FIB, COL_I, and COL_{IV} nanofabrics were engineered as linear (Figure 2m−o) and interconnected fibrillar networks (Figure 2p). This illustrates the range of ECM proteins that can be engineered with spatial dimensions and hierarchal architectures that exceed those obtainable with microfluidics[34] or entropy-driven assembly[14] of COL_I, FIB, and Matrigel (LAM, COL_{IV}, and entactin) gels. As a control experiment, the polysaccharide dextran was patterned onto PIPAAm and released but dissolved into solution and did not assemble into an insoluble matrix (see Supporting Information, Figure S2 and Movie S4). Additionally, control experiments using the proteins bovine serum albumin (BSA) and Immunoglobulin G (IgG) patterned onto PIPAAm and released (Supporting Information, Figure S3a and S3b, respectively) failed to form nanofabrics. When we attempted to make nanofabrics with BSA and IgG, they broke into small fragments and short fibrils during release. This suggests that nanofabric formation requires biopolymers with intrinsic self-binding, fibrillogenesis domains. Further, nanofabric

DOI: 10.1021/nl100998p | *Nano Lett.* **2010,** *10,* 2184--2191

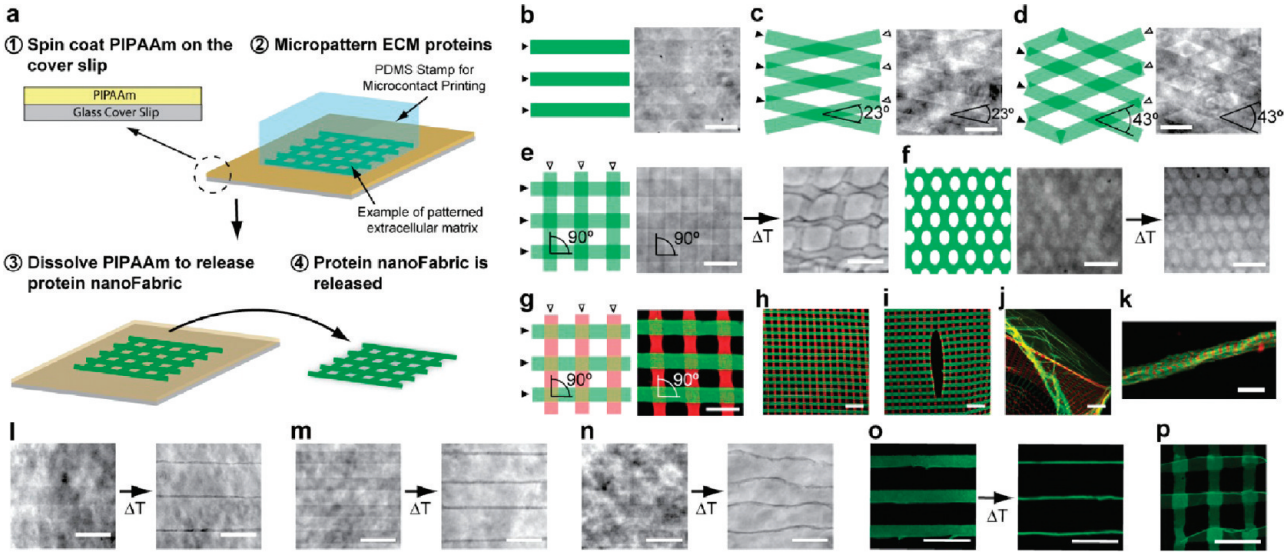

FIGURE 2. Fabrication of protein nanofabrics and example architectures and compositions. (a) Schematic of the nanofabric fabrication process. (b) Schematic and example optical phase image of 20 × 20 FN lines μCP onto PIPAAm. (c−e) The 20 × 20 FN lines were serially microcontact printed onto PIPAAm at angles of 23, 43, and 90° (c, d, and e, respectively). (e) The 20 × 20 FN lines, crossed at 90°, maintain the patterned microstructure following thermal release. (f) A single stamping may have a more complex structure than lines, as demonstrated by this "fish net" pattern with ~20 μm wide elliptical holes. (g) The 20 × 20 lines of LAM (red, vertical lines) and FN (green, horizontal lines) were serially printed onto PIPAAm demonstrating that an integrated protein nanofabric can consist of multiple ECM proteins. (h) The bicomponent FN and LAM nanofabric maintains its microstructure upon thermal release, (i) can support small tears without failing, (j) can be formed as continuous protein films, or (k) can be rolled into fibers. (l) The 20 × 20 LAM lines μCP onto PIPAAm and after thermal release. (m) The 15 × 15 FIB lines μCP onto PIPAAm and after thermal release. (n) The 15 × 15 COL_{IV} lines μCP onto PIPAAm and after thermal release. (o) The 20 × 20 COL_I lines μCP onto PIPAAm and after thermal release. (p) The 20 × 20 COL_I lines crossed at 90° and μCP onto PIPAAm. Scale bars are 40 μm for (b−g and l−p) and 100 μm for (h−k).

formation is not due to residual PIPAAm potentially trapped during thermal release, as the PIPAAm is below its lower critical solution temperature (22 °C) and thus highly hydrated and nonprotein binding. Even though the ECM proteins we investigated have different receptor-mediated and enzymatic-based assembly processes in vivo, nanofabrics could be engineered in vitro from FN, LAM, FIB, COL_I, and COL_{IV}, thus providing a new way to create multiscale structures from the major ECM proteins.

Nanofabrics contracted during release from the PIPAAm, and we explored this apparent prestress by analyzing how FN, LAM, FIB, COL_I, and COL_{IV} fabrics recoiled in the longitudinal and transverse directions (Figure 3). For example, 20 × 20 FN nanofabric lines released from PIPAAm rapidly contracted from a patterned width of 20 μm to a reduced width of ~3 μm (Figure 3a, Supporting Information, Movies S1 and S2). The PIPAAm layer expands as it hydrates and dissolves, so this nanofabric contraction occurs in the opposite direction. We propose that this prestress is caused by a conformational change in the FN molecules from the unfolded, surface-adsorbed conformation[23,24] to a more globular, solution-like conformation upon release. This response could be modulated by creating interconnected, fibrillar architectures, which formed prestressed networks that limited protein refolding, comparable to the prestress in cell-generated matrix[35] (Figures 3b, 2e,g, Supporting Information, Movie S3). Nanofabrics composed of FN, LAM, FIB, COL_I, and COL_{IV} exhibited similar prestress and contraction upon release. The degree to which the different ECM proteins refolded after release was estimated from the change in lateral dimension of linear, ribbonlike 20 × 20 nanofabric lines (Figure 3c). The contraction of the FN structures depicted in Figure 3a suggests that patterned FN molecules were unfolded approximately 6-fold relative to the contracted (released) state. The other ECM proteins displayed similar behavior with FIB, COL_I, and COL_{IV} unfolding approximately 5-fold and LAM unfolding approximately 8-fold. Protein adsorption to hydrophobic PDMS surfaces is nonspecific, one explanation for the similar unfolding of the different ECM proteins. Once released, nanofabrics could be stretched repeatedly demonstrating that this apparent folding and unfolding was reversible, similar to cell-generated ECM.[35]

To understand how conformational changes in the proteins may affect the structural and mechanical properties, we focused our characterization on FN nanofabrics. Thickness was customized by controlling the density of protein molecules adsorbed to the surface via the concentration of the FN solution used to ink the μCP PDMS stamp (Figure 3d,e). Dry FN nanofabrics on PIPAAm were 1−5 nm thick (Figure 3f), comparable to FN dimers unfolded on hydrophobic and hydrophilic mica surfaces.[23,27] The FN nanofabric thickness increased to ~8 nm when hydrated, significantly less than the FN dimer diameter in solution.[36] This thickness limit of <10 nm is in the range of a molecular layer, further suggestive of nanofabric formation being driven by

DOI: 10.1021/nl100998p | *Nano Lett.* **2010,** *10,* 2184--2191

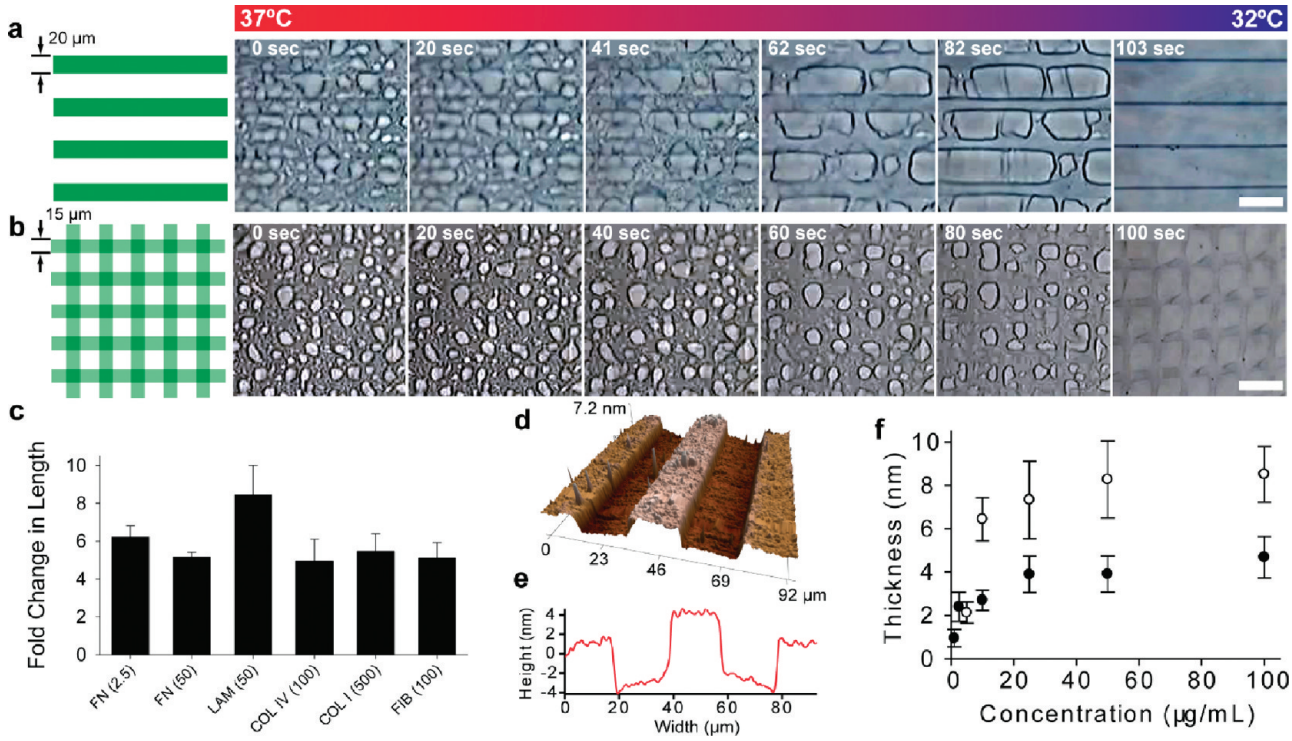

FIGURE 3. Thermal release of protein nanofabrics from PIPAAm and the dimensional changes due to nanofabric contraction. (a) Thermal release of 20 × 20 FN nanofabric lines results in contraction and dimensional change as the PIPAAm hydrates and dissolves. (b) The thermal release of 20 × 20 FN lines printed at 90° demonstrates that the square lattice structure supports the prestress and reduces dimensional change of the nanofabric upon release. (c) The fold change in linear nanofabric width prerelease versus postrelease for FN, LAM, FIB, COL_I, and COL_{IV} (protein concentration given in parentheses in μg/mL). Note that concentration of FN does not significantly alter degree of folding. (d) AFM scan of 20 × 20 FN nanofabric lines on PIPAAm and (e) the corresponding cross-sectional profile. (f) FN nanofabric thickness varied as a function of concentration of FN and whether the nanofabric was dry (●) or hydrated (○). Scale bars are 40 μm for (a,b). Error bars in (c,f) are standard deviation.

direct protein/surface interactions. The relative change in nanofabric dimensions upon release suggests that constituent proteins and their folding properties influence the mechanical properties.

Free-standing FN nanofabrics captured on PDMS substrates (Figure 4a) had a dense network of interconnected fibrils (Figure 4b), structurally similar to force-induced FN matrix assembly.[20] By cross section, these fibrils were <100 nm in width (Figure 3c), indicating that some fibrils might be composed of multiple FN dimers (2 to 3 nm wide[36]) in parallel. Contracted 20 × 20 FN fibers (Figure 4d) showed the formation of a nodular nanostructure with a higher density at the edges (Figure 4f) than in the center (Figure 4e), but with an equivalent diameter of ~55 nm for both regions. This diameter is comparable to FN dimers in solution (~50 nm),[36] but smaller than nodules in cell-generated[37] and surface-tension-induced[20] FN matrices, attributed to the refolding of FN type III domains during fibril relaxation.[38] Many nodules in the lower density region (Figure 4e) were arranged in a line like "beads-on-a-string" and oriented orthogonally to the fiber axis, as if under a tension, between the higher density regions. These differences in nodule density were not due to folding over of the nanofabric on to itself. For example, a 20 × 20 FN line in a partially contracted state (Figure 4g) had a uniform density of nodules from its center to one edge (Figure 4i) that transitioned to a higher density edge region as the overall width of the nanofabric decreased (Figure 4h). One possible explanation is that the nodules are single or small-numbers of folded or partially folded FN dimers connected together by unfolded FN dimers not resolved by SEM. Further, the smallest subunit of the nanofabric appeared to be single nodules (Figure 4j), consistent with the interpretation that the nodules in contracted nanofabrics are folded dimers. When a nanofabric did fold over on itself it was easy to identify (Figure 4k), because the nanofabric looked similar to folds in a fishing net (Figure 4l).

We performed mechanical testing to determine if the FN nanofabric deformation was reversible. Nanofabrics were released onto a PDMS support and then a micromanipulator with a PDMS coated tip was used to grab the nanofabric via hydrophobic, nonspecific binding and apply uniaxial strain (Supporting Information, Figure S4a). For example, linear nanofabric strands could be reversibly stretched 4.39-fold from the contracted state, a 1D Lagrange strain of 912% (Supporting Information, Figure S4b–f and Movie S6, reversed in Figure S4g,h). Stretch ratios up to 5.92 were measured before failure (Supporting Information, Figure S5), but it was not possible to determine if the nanofabric adhesion to the micromanipulator tip failed or if the nano-

DOI: 10.1021/nl100998p | *Nano Lett.* **2010,** *10,* 2184–2191

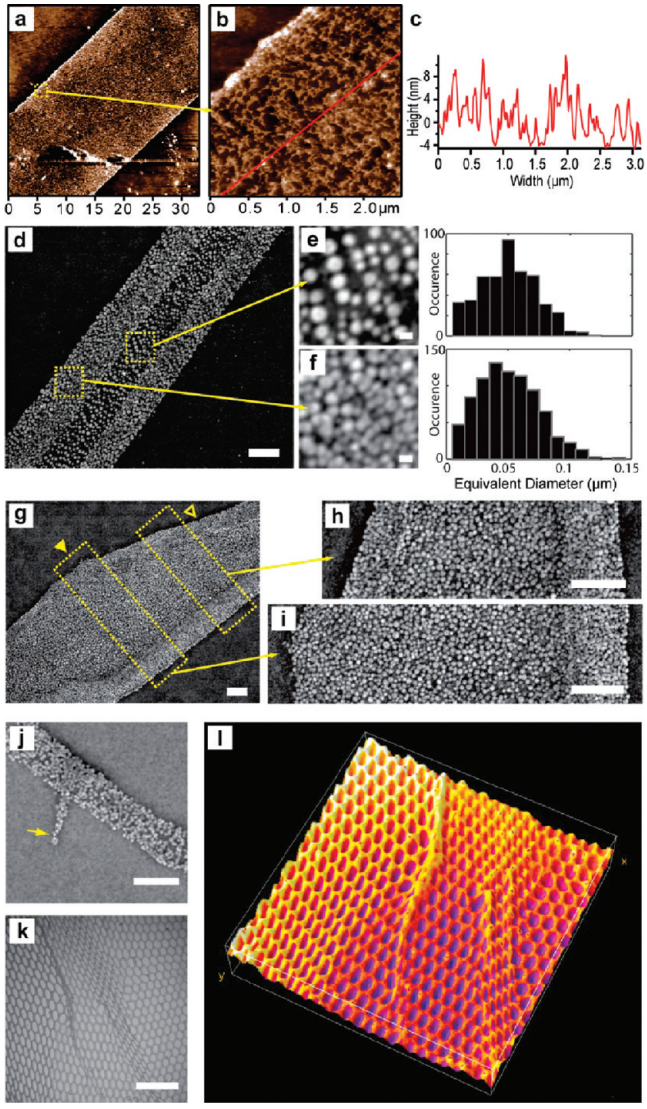

FIGURE 4. Ultrastructural analysis of FN nanofabrics reveals the transition from a fibrillar to nodular structure upon release and contraction. (a) FN 20 × 20 line nanofabric transferred to PDMS during release preserves *XY* dimensions (as imaged by AFM in phosphate buffered saline). (b) A high-resolution scan shows a fibrillar architecture and a cross section (c) reveals these fibrils are <10 nm thick. (d) FN 20 × 20 line nanofabric released and imaged by SEM, the ~3.2 μm width is similar to that when hydrated (Figure 3a), indicating that dehydration and coating for SEM did not alter dimensions. The released nanofabric is composed of nanoscale nodules in (e) high-density regions on the edges and (f) a low-density region in the center, but the equivalent diameters show similar distributions centered at ~50 nm. (g) The bottom edge of a FN 20 × 20 line has a ~1 μm wide high-density region as in (d), but the top edge transitions from low-density packing (yellow ▼ and h) to higher-density packing (yellow ▽ and i). (j) FN nanofabrics after release showed that the smallest observable fragments were nodules ~50 nm in diameter, consistent with refolded FN dimers. (k) Folded nanofabrics appeared different than the high-density regions, evident in the "netlike" ripples of a FN nanofabric with elliptical pores. (l) A three-dimensional surface rendering of (k) demonstrates that ripples and folds are qualitatively similar to those observed in macroscale fishing nets (*X*, *Y* axes are 360 μm). Scale bars are 1 μm for (d,g,h,i,j); 100 nm for (e,f); 100 μm for (j).

fabric ripped. Using the micromanipulator, the 2D nanofabrics could be reversibly stretched up to ~3-fold (Supporting Information, Figure S6 and Movie S7) with adhesive failure between the nanofabric and micromanipulator tip preventing larger strains from being applied. We measured the width of FN fibers in nanofabrics prior to and after thermal release and in the contracted and stretched free-standing nanofabrics. These data showed that constituent FN strands underwent concomitant deformation (Supporting Information, Figure S7). This is important because it demonstrates that the FN nanofabrics have consistent mechanical properties across adjacent strands.

Review of the literature suggested that our experimental technique was limiting our ability to measure the full range of nanofabric extensibility. The FN dimer is 51 × 32 nm in solution[36] and the contour length is ~160 nm, a maximum 3- to 5-fold change if tertiary structure is lost and secondary structure is preserved. The FN type III domain is β-sheet rich (stores mechanical energy,[6,39]) and unfolding the secondary structure of one of the 30 type III repeats increases the contour length by ~28.5 nm.[40] On the basis of these previous reports, we calculated that unfolding all tertiary and secondary type III structure would increase the contour length to ~1015 nm, an ~18-fold change relative to the dimer in solution.

To test this prediction, we employed an alternative technique to measure the extensibility of the nanofabrics.[20] Surface tension from evaporating water droplets was used to repeatedly adhere nanofabrics composed of 20 × 20 FN lines to glass coverslips in a stretched state. (Figure 5a,b, Supporting Information, Movie S5) Stretching along the horizontal axis of the nanofabric (Figure 5c) revealed an increase in pitch from the patterned 40 μm to 102 ± 20 μm, a stretch ratio of 2.55. However, the patterned nanofabric contracts when it is released from the PIPAAm, and so to determine the total range of nanofabric deformation we need to consider dimensional changes relative to the fully contracted state. To do this we examined the width of individual nanofabric strands within the 2D nanofabric (Figure 5d). Horizontal strands were laterally contracted (~3 μm wide) and vertical strands were laterally stretched (~45 μm wide), approximately a 15-fold deformation and in reasonable agreement with our calculations. This observation may be attributed to the nodular structure in the contracted FN nanofabric and fibrillar structure in the stretched FN nanofabric, as AFM analysis revealed comparable nodular and fibrillar nanostructures (Figure 5e–j). Contracted regions had high nodular density, and stretched regions had lower nodular density (Figure 5f,g). AFM-resolved fibrillar structures connecting nodules together (Figure 5h) and the same "bead-on-a-string" structures observed by SEM oriented in the direction of mechanical strain (Figure 5i). Closer examination of the region between nodules revealed a fibrous meshwork interconnecting them, consistent in height and diameter with unfolded FN dimers.

DOI: 10.1021/nl100998p | *Nano Lett.* **2010,** *10,* 2184–2191

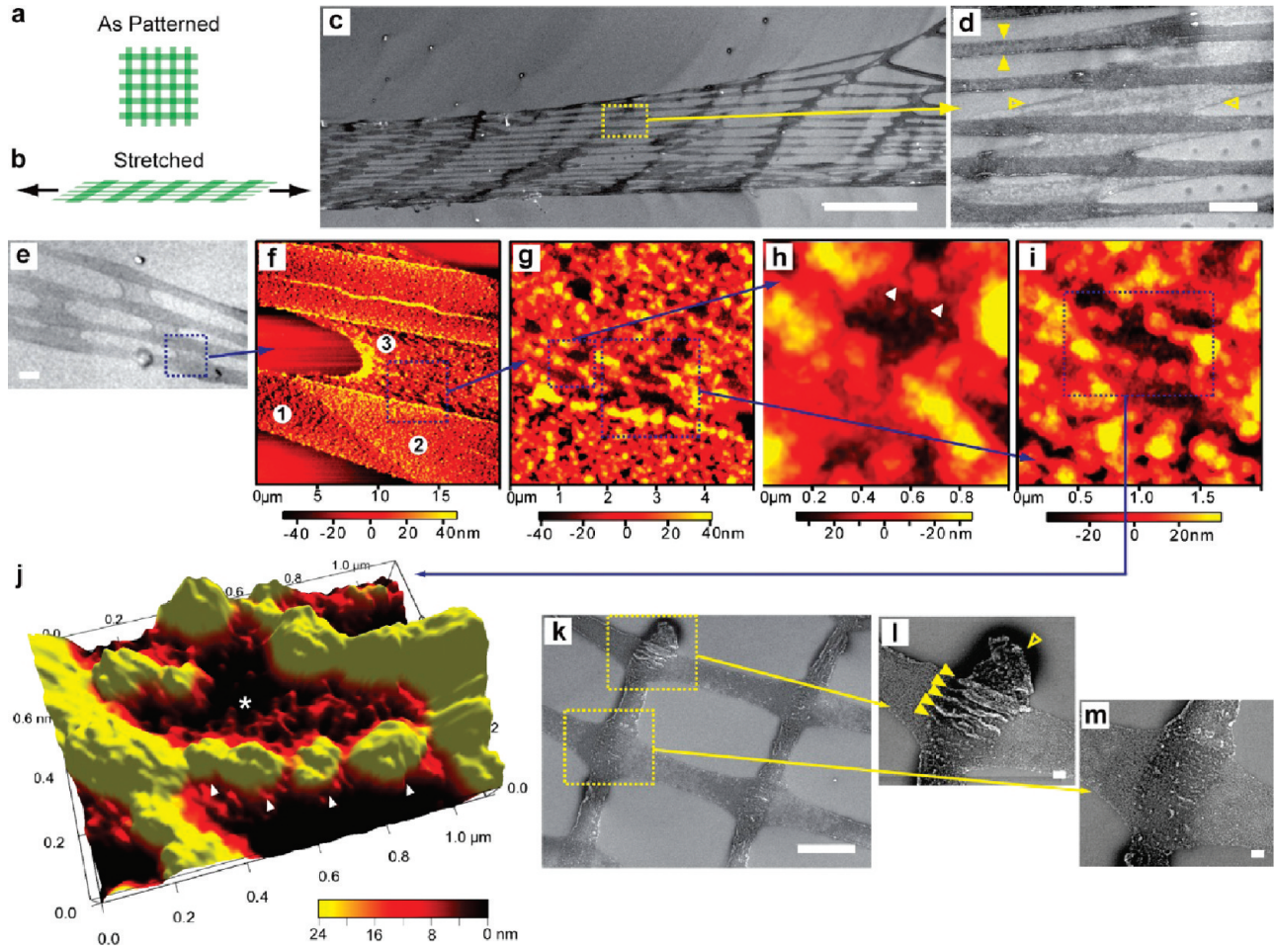

FIGURE 5. Stretched FN nanofabrics are highly extensible with a nodular/fibrillar change in nanostructure under strain. (a) Schematic of a nanofabric composed of FN 20 × 20 lines at 90° before release and (b) stretched postrelease. (c) SEM image of a FN nanofabric stretched longitudinally demonstrating that large strains are supported. (d) Zoomed region from (c) shows that the horizontal lines (yellow ▼) have contracted to ~3 μm wide while the vertical lines (yellow ▽) have been stretched to ~45 μm wide, a 15-fold difference. (e) Optical image of a stretched nanofabric, a section of which was imaged by AFM. (f) Region (1) shows the high-density nodular nanostructure of the horizontal lines that have contracted laterally to ~5 μm. Region (2) shows the higher-density nodules where the horizontal and vertical lines overlap. Region (3) shows the low-density nodules and fibrillar appearance of the vertical lines stretched between two lateral lines. (g) Zoomed region from (f) reveals the transition in nodular structure from the overlap region to the more fibrillar region. (h) Zoomed region from (g) reveals what appears to be stretched fibrils (white ▼) connecting two larger nodules with a smaller nodule in-between. (i) Zoomed region from (g) illustrates the linear arrangement of nodules like "beads-on-a-string" aligned in the direction of stretch suggesting these nodules are coupled by unfolded FN. (j) A 3D rendering from the region in (i) emphasizes the nodular structure (white ▼) and a region (as denoted by white "☆") that contains a meshwork of smaller fibrils running between nodules. Nodule diameter is consistent with folded and partially refolded FN dimers and the height of the fibrils connecting the nodules is consistent with unfolded FN dimers. (k) Prestress in the stretched FN nanofabrics is confirmed by examining the morphology at points of failure. (l) Rupture of a FN 20 × 20 line (yellow ▽) reveals an apparent 3-fold contraction from an initial length of ~15 μm to ~5 μm. The compressive stress from the failure is sufficient to cause periodic buckling (yellow ▼) in the underlying, orthogonal nanofabric. (m) An intact orthogonal junction. Scale bars are 100 μm for (c); 10 μm for (d,e,k); 1 μm for (l,m).

During mechanical failure, when a microscale section of interconnected FN nanofabric ruptured it contracted to one-fourth its length (Figure 5k,l), comparable to failure of FN fibrils in cell-assembled matrices that contract to one-third to one-fourth the initial length.[35] Thus, it appears that for both FN nanofabrics and cell-generated FN ECM, the prestressed network can support local failures by protein refolding and fiber buckling. This buckling (Figure 5 panel l, compared to panel m) indicates that the effective elastic modulus of the prestressed, upper region was many times greater than that of the contracted, lower region of the nanofabric.[41] These data suggest that FN and the other ECM protein nanofabrics are capable of multiscale deformation via a combination nanoscale molecular folding, microscale buckling and macroscale fabric architecture, which, if appropriately leveraged, could lead to the development of advanced, high-performance textiles[42] and protein-based materials.

To assess biological functionality, we investigated the interaction of nanofabrics with cells by engineering beating cardiac muscle. In engineered myocardium, it is critical to align and support the ECM to maintain tissue structure, ensure matrix stability under cell-generated forces and facilitate the mechanochemical coupling that enables cellular

DOI: 10.1021/nl100998p | Nano Lett. 2010, 10, 2184--2191

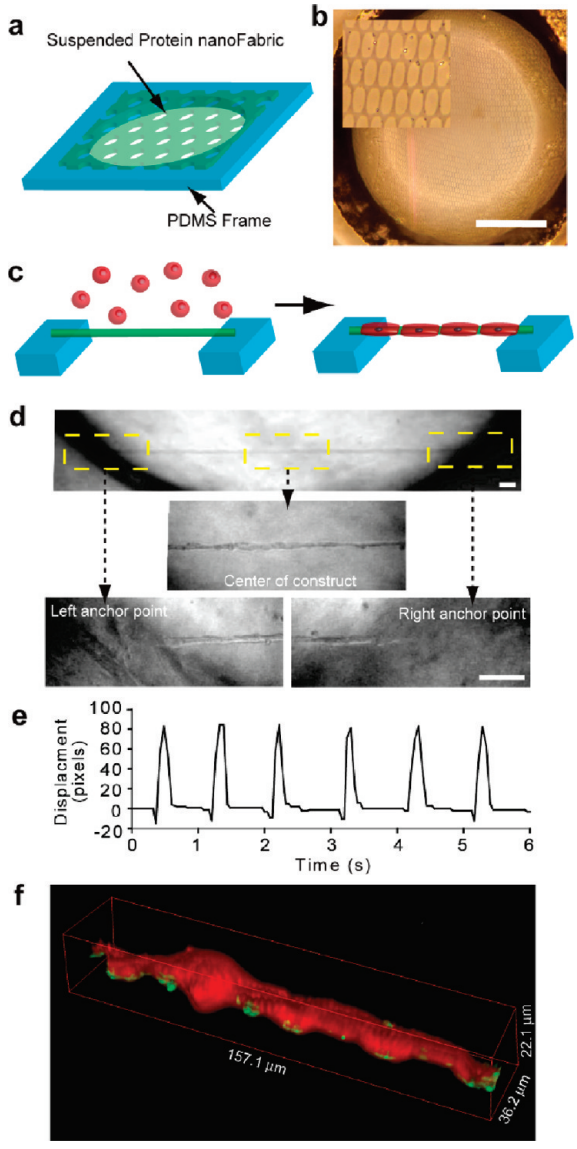

FIGURE 6. Tissue engineering myocardium using protein nanofabrics. (a) Schematic of nanofabrics supported by a frame of PDMS where the nanofabric spans the opening in the PDMS. (b) Example of a netlike FN nanofabric supported by a PDMS frame across a millimeter-scale opening (stitched multiple fields of view), inset shows higher magnification image. (c) Schematic of a single, FN nanofabric thread supported by a PDMS frame and seeded with cardiomyocytes that bind to the FN and assemble into a myocardial strand. (d) A papillary musclelike strand of myocardium with higher-magnification images of the left anchor, center, and right anchor regions was approximately 20 μm wide and 2 mm long suspended at the ends to a PDMS frame. The FN nanofabric thread upon which the cardiomyocytes are bound was 20 μm wide, 2 mm long and ~8 nm thick when patterned. (e) Plot of pixel displacement as the myocardial strand beats at ~1 Hz. (f) Cardiomyocytes were cultured on FN nanofabrics and then fixed and stained to demonstrate cell attachment; stained for F-actin (red) and FN (green). Scale bars are 1 mm (c) and 100 μm (d).

function. To create free-standing nanofabrics, we designed PDMS frames to support one-dimensional strands and two-dimensional FN nanofabrics (Figure 6a–d). Nanofabrics were mechanically stable under their own weight at the millimeter length-scale (Figure 6b). Cardiomyocytes passively seeded and cultured on a nanofabric adhered and spontaneously aligned with respect to the underlying matrix, demonstrating that FN nanofabrics can bind cells, direct cell–cell electromechanical coupling, uniaxially orient the contractile cytoskeleton[13,28] and mechanically support cyclic contraction over several days in culture (Figure 6d,e, and Supporting Information, Movie S8). This is important because it establishes that a free-standing, fibrillar FN scaffold can be engineered to maintain structural integrity during myogenesis and bear cyclic, biomechanical loading. A 3D reconstruction of cardiomyocytes on a FN nanofabric adhered to a PDMS substrate confirms the capability to guide anisotropic myogenesis (Figure 6f).

No cytotoxicity was associated with the nanofabric due to possible residual PIPAAm. For example, centimeter-scale anisotropic cardiac muscle was engineered by culturing cardiomyocytes on FN nanofabric networks, while still adhered to PIPAAm (Supporting Information, Figure S8, Movies S9,S10), similar to cell-sheet engineering approaches;[32,33,43] however with nanofabrics the engineered ECM is released with the cells.[44] Cardiomyocytes cultured on these PIPAAm-bound nanofabrics were viable for nearly a week prior to release (Supporting Information, Figure S8). These results suggest that nanofabrics could be used in the modular assembly of anisotropic tissues without the need for synthetic scaffold materials, which either fail to degrade[13] or leave heterogeneities that are potentially arrhythmogenic and reduce force generation.[45,46]

In summary, we can use surface-initiated assembly to engineer multiscale, free-standing nanofabrics using a variety of ECM proteins (FN, LAM, FIB, COL_I, and COL_{IV}). This process exploits soft lithography to tailor chemical and mechanical anisotropy and a thermally sensitive substrate to enable nondestructive protein release. FN nanofabrics have unique mechanical properties that outperform synthetic polymers, potentially leading to a new class of advanced, high-performance biomolecular materials. For tissue engineering, protein nanofabrics offer distinct advantages over ECM gels, synthetic scaffolds,[47] and cell-sheets by providing spatially encoded guidance cues in a bioactive and bioresorbable matrix. Engineered cardiac muscle demonstrated the ability of the nanofabrics to functionally organize cells into an anisotropic tissue, including papillary musclelike cell threads. The protein nanofabrics did not degrade during these cell studies suggesting their stability for tissue engineering. However, nanofabrics have the potential for longer-term remodeling, as the constituent proteins have similar biochemical and biomechanical properties to native ECM.

Acknowledgment. We acknowledge financial support from the DARPA Biomolecular Motors Program, the Air Force Office of sponsored research, and the Harvard Materials Research Science and Engineering Center (MRSEC). We thank Katherine Scholtz for her assistance in obtaining the scanning electron microscope data, Asylum Research for assistance in obtaining some of the atomic force microscopy

DOI: 10.1021/nl100998p | *Nano Lett.* **2010,** *10,* 2184–2191

data, Sean P. Sheehy for assistance with the cardiomyocyte harvest and the Harvard Center for Nanoscale Systems (CNS) for use of their cleanroom facilities.

Supporting Information Available. Experimental methods, Figures S1−S8, and videos S1−10. This material is available free of charge via the Internet at http://pubs.acs.org.

REFERENCES AND NOTES

(1) Mao, Y.; Schwarzbauer, J. E. *Matrix Biol.* **2005**, *24* (6), 389–399.
(2) Schwarzbauer, J. E.; Sechler, J. L. *Current Opin. Cell Biol.* **1999**, *11* (5), 622–627.
(3) Wu, C.; Keivens, V. M.; O'Toole, T. E.; McDonald, J. A.; Ginsberg, M. H. *Cell* **1995**, *83*, 715–724.
(4) Vogel, V.; Sheetz, M. *Nat. Rev. Mol. Cell Biol.* **2006**, *7* (4), 265–275.
(5) Geiger, B.; Bershadsky, A.; Pankov, R.; Yamada, K. M. *Nat. Rev. Mol. Cell Biol.* **2001**, *2* (11), 793–805.
(6) Bao, G.; Suresh, S. *Nat. Mater.* **2003**, *2* (11), 715–725.
(7) Sakai, T.; Larsen, M.; Yamada, K. M. *Nature* **2003**, *423* (6942), 876–881.
(8) Leask, A.; Abraham, D. J. *FASEB J.* **2004**, *18* (7), 816–827.
(9) Chien, K. R.; Domian, I. J.; Parker, K. K. *Science* **2008**, *322* (5907), 1494–1497.
(10) Gurtner, G. C.; Werner, S.; Barrandon, Y.; Longaker, M. T. *Nature* **2008**, *453* (7193), 314–321.
(11) Ott, H. C.; Matthiesen, T. S.; Goh, S.-K.; Black, L. D.; Kren, S. M.; Netoff, T. I.; Taylor, D. A. *Nat. Med.* **2008**, *14* (2), 213–221.
(12) Dallas, S. L.; Chen, Q.; Sivakumar, P.; Gerald, P. S. Dynamics of Assembly and Reorganization of Extracellular Matrix Proteins. In *Current Topics in Developmental Biology*; Academic Press: New York, 2006; Vol. 75, pp 1−24.
(13) Feinberg, A. W.; Feigel, A.; Shevkoplyas, S. S.; Sheehy, S.; Whitesides, G. M.; Parker, K. K. *Science* **2007**, *317* (5843), 1366–1370.
(14) Kadler, K. E.; Hill, A.; Canty-Laird, E. G. *Curr. Opin. Cell Biol.* **2008**, *20* (5), 495–501.
(15) Mosher, D. F.; Johnson, R. B. *J. Biol. Chem.* **1983**, *258* (10), 6595–6601.
(16) Sakai, K.; Fujii, T.; Hayashi, T. *J Biochem.* **1994**, *115* (3), 415–421.
(17) Baneyx, G.; Vogel, V. *Proc. Natl. Acad. Sci. U.S.A.* **1999**, *96* (22), 12518–12523.
(18) Little, W. C.; Smith, M. L.; Ebneter, U.; Vogel, V. *Matrix Biol.* **2008**, *27* (5), 451–461.
(19) Klotzsch, E.; Smith, M. L.; Kubow, K. E.; Muntwyler, S.; Little, W. C.; Beyeler, F.; Gourdon, D.; Nelson, B. J.; Vogel, V. *Proc. Natl. Acad. Sci. U.S.A.* **2009**, *106* (43), 18267–18272.
(20) Ulmer, J.; Geiger, B.; Spatz, J. P. *Soft Matter* **2008**, *4* (10), 1998–2007.
(21) Ahmed, Z.; Underwood, S.; Brown, R. A. *Tissue Eng.* **2003**, *9* (2), 219–231.
(22) Kaiser, P.; Spatz, J. P. *Soft Matter* **2010**, *6*, 113–119.
(23) Bergkvist, M.; Carlsson, J.; Oscarsson, S. *J. Biomed. Mater. Res.* **2003**, *64A* (2), 349–356.
(24) Baugh, L.; Vogel, V. *J. Biomed. Mater. Res., Part A* **2004**, *69A* (3), 525–534.
(25) Barber, T. A.; Mathis, T.; Ihlenfeld, J. V.; Cooper, S. L.; Mosher, D. F. *Scanning Electron Microsc.* **1978**, (2), 431–440.
(26) Chen, Y.; Wu, Y.; Cai, J. *Biochem. Biophys. Res. Commun.* **2007**, *361* (2), 391–397.
(27) Hull, J. R.; Tamura, G. S.; Castner, D. G. *Biophys. J.* **2007**, *93* (8), 2852–2860.
(28) Parker, K. K.; Tan, J.; Chen, C. S.; Tung, L. *Circ. Res.* **2008**, *103* (4), 340–342.
(29) Parker, K. K.; Brock, A. L.; Brangwynne, C.; Mannix, R. J.; Wang, N.; Ostuni, E.; Geisse, N. A.; Adams, J. C.; Whitesides, G. M.; Ingber, D. E. *FASEB J.* **2002**, *16* (10), xxxx.
(30) Nie, Z.; Kumacheva, E. *Nat. Mater.* **2008**, *7* (4), 277–290.
(31) Bray, M.-A.; Sheehy, S. P.; Parker, K. K. *Cell Motil. Cytoskeleton* **2008**, *65* (8), 641–651.
(32) Akiyama, Y.; Kikuchi, A.; Yamato, M.; Okano, T. *Langmuir* **2004**, *20* (13), 5506–5511.
(33) Canavan, H. E.; Cheng, X.; Graham, D. J.; Ratner, B. D.; Castner, D. G. *Langmuir* **2005**, *21* (5), 1949–1955.
(34) Gillette, B. M.; Jensen, J. A.; Tang, B.; Yang, G. J.; Bazargan-Lari, A.; Zhong, M.; Sia, S. K. *Nat. Mater.* **2008**, *7* (8), 636–640.
(35) Ohashi, T.; Kiehart, D. P.; Erickson, H. P. *Proc. Natl. Acad. Sci. U.S.A.* **1999**, *96* (5), 2153–2158.
(36) Erickson, H. P.; Carrell, N. A. *J. Biol. Chem.* **1983**, *258* (23), 14539–14544.
(37) Peters, D. M.; Portz, L. M.; Fullenwider, J.; Mosher, D. F. *J. Cell Biol.* **1990**, *111* (1), 249–256.
(38) Peters, D. M. P.; Chen, Y.; Zardi, L.; Brummel, S. *Microsc. Microanal.* **1998**, *4* (4), 385–396.
(39) Sotomayor, M.; Schulten, K. *Science* **2007**, *316* (5828), 1144–1148.
(40) Oberhauser, A. F.; Badilla-Fernandez, C.; Carrion-Vazquez, M.; Fernandez, J. M. *J. Mol. Biol.* **2002**, *319* (2), 433–447.
(41) Stafford, C. M.; Harrison, C.; Beers, K. L.; Karim, A.; Amis, E. J.; Vanlandingham, M. R.; Kim, H. C.; Volksen, W.; Miller, R. D.; Simonyi, E. E. *Nat. Mater.* **2004**, *3* (8), 545–550.
(42) Sanchez, C.; Arribart, H.; Giraud Guille, M. M. *Nat. Mater.* **2005**, *4* (4), 277–288.
(43) Shimizu, T.; Yamato, M.; Isoi, Y.; Akutsu, T.; Setomaru, T.; Abe, K.; Kikuchi, A.; Umezu, M.; Okano, T. *Circ. Res.* **2002**, *90* (3), No. E40−E48.
(44) Williams, C.; Tsuda, Y.; Isenberg, B. C.; Yamato, M.; Shimizu, T.; Okano, T.; Wong, J. Y. *Adv. Mater.* **2008**, *21* (21), 2161–2164.
(45) Engelmayr, G. C.; Cheng, M.; Bettinger, C. J.; Borenstein, J. T.; Langer, R.; Freed, L. E. *Nat. Mater.* **2008**, *7*, 1003–1010.
(46) Christman, K. L.; Lee, R. J. *J. Am. Coll. Cardiol.* **2006**, *48* (5), 907–913.
(47) Mitragotri, S.; Lahann, J. *Nat. Mater.* **2009**, *8* (1), 15–23.

DOI: 10.1021/nl100998p | *Nano Lett.* **2010,** *10,* 2184--2191